AGU PUBLICATIONS

Geophysical Research Letters

RESEARCH LETTER
10.1002/2016GL068375

Key Points:
- A framework for kinematically consistent viscoelastic stress through the earthquake cycle is presented
- In the models, earthquake-generated stresses are zero at the end of the earthquake cycle and may reach an interseismic maximum
- Based on the timing of stress maxima, the mean time of viscoelastically triggered earthquakes may be ~5–35% through the earthquake cycle

Correspondence to:
P. M. R. DeVries,
phoeberobinson@fas.harvard.edu

Citation:
DeVries, P. M. R., and B. J. Meade (2016), Kinematically consistent models of viscoelastic stress evolution, *Geophys. Res. Lett.*, *43*, 4205–4214, doi:10.1002/2016GL068375.

Received 23 FEB 2016
Accepted 5 APR 2016
Accepted article online 7 APR 2016
Published online 4 MAY 2016

Kinematically consistent models of viscoelastic stress evolution

Phoebe M. R. DeVries[1] and Brendan J. Meade[1]

[1]Department of Earth and Planetary Sciences, Harvard University, Cambridge, Massachusetts, USA

Abstract Following large earthquakes, coseismic stresses at the base of the seismogenic zone may induce rapid viscoelastic deformation in the lower crust and upper mantle. As stresses diffuse away from the primary slip surface in these lower layers, the magnitudes of stress at distant locations (>1 fault length away) may slowly increase. This stress relaxation process has been used to explain delayed earthquake triggering sequences like the 1992 $M_w = 7.3$ Landers and 1999 $M_w = 7.1$ Hector Mine earthquakes in California. However, a conceptual difficulty associated with these models is that the magnitudes of stresses asymptote to constant values over long time scales. This effect introduces persistent perturbations to the total stress field over many earthquake cycles. Here we present a kinematically consistent viscoelastic stress transfer model where the total perturbation to the stress field at the end of the earthquake cycle is zero everywhere. With kinematically consistent models, hypotheses about the potential likelihood of viscoelastically triggered earthquakes may be based on the timing of stress maxima, rather than on any arbitrary or empirically constrained stress thresholds. Based on these models, we infer that earthquakes triggered by viscoelastic earthquake cycle effects may be most likely to occur during the first 50% of the earthquake cycle regardless of the assumed long-term and transient viscosities.

1. Introduction

Elastic stress changes due to large earthquakes have been used to explain geographical patterns of aftershocks [e.g., *Hardebeck et al.*, 1998; *King et al.*, 1994] and earthquake sequences [e.g., *Stein et al.*, 1997; *Doser and Robinson*, 2002; *Parsons and Dreger*, 2000; *Nalbant et al.*, 1998; *King and Cocco*, 2001] in the western U.S., Turkey, New Zealand, the Aegean Sea, and many other tectonic settings worldwide. Elastic Coulomb failure stress changes ($\Delta CFS_{elastic}$) are particularly widely used to map locations at which the occurrence of future earthquakes may be either encouraged or suppressed by the effects of past earthquakes [e.g., *King et al.*, 1994; *Harris*, 1998; *Steacy et al.*, 2005]. In the Coulomb failure criterion framework, seismic slip occurs on a given plane when the Coulomb failure stress σ_f is greater than

$$\sigma_f = \tau - \mu' \sigma_n \tag{1}$$

where τ is the shear stress on the failure plane, σ_n is the normal stress, and μ' is the effective coefficient of friction [e.g., *King et al.*, 1994]. The effective coefficient of friction, μ', depends on the assumption that fluid pressure is linearly related to the confining stress on the failure plane [e.g., *Harris*, 1998; *Simpson and Reasenberg*, 1994].

However, elastic Coulomb failure stress changes cannot account for patterns of triggered earthquakes in every case. After some earthquakes, like the 1994 Northridge earthquake in California, regions of elevated $\Delta CFS_{elastic}$ are not well correlated with aftershock locations [*Hardebeck et al.*, 1998]. Perhaps most importantly, elastic Coulomb failure stress changes occur instantaneously after a large earthquake, and thus cannot easily explain time delays of years to decades between a triggering event and potentially triggered events, such as those observed during the 1939–1999 earthquake sequence in Turkey [e.g., *Stein et al.*, 1997]. Time-dependent frictional properties may help to explain these observed time delays [e.g., *Dieterich*, 1992, 1994; *Stein et al.*, 1997].

Models that incorporate time-dependent viscoelastic stress changes may also explain time delays of years to decades between a triggering earthquake and a triggered earthquake [e.g., *Freed and Lin*, 2001; *Zeng*, 2001; *Pollitz and Sacks*, 2002]. In these models, slip on a fault induces large stresses in the viscoelastic lower crust and upper mantle beneath, which may flow over time to relax these stresses. This relaxation process may lead to significant time-dependent changes in stress (up to 10 times as large in magnitude as elastic stress

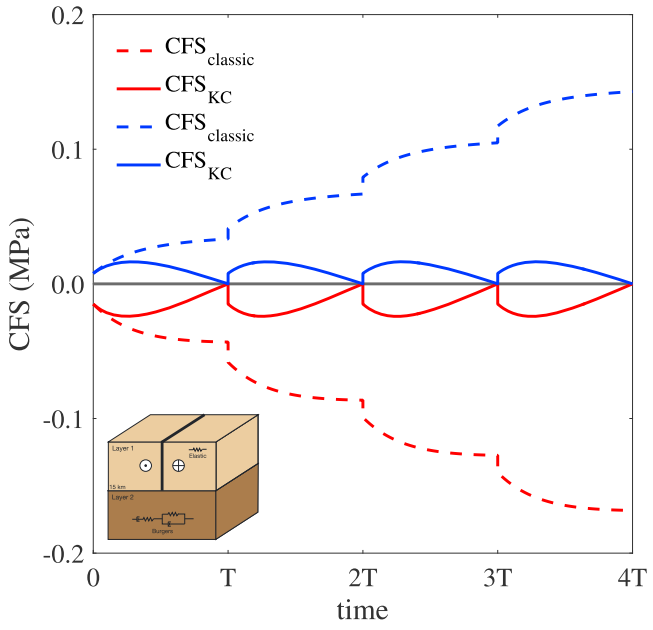

Figure 1. The evolution of $\Delta CFS_{classic}$ (Figure 2, row 1) and ΔCFS_{KC} (Figure 2, row 2) at two specific locations over many earthquake cycles. In this example calculation, $T = 100$ years with a two-layer Burgers model ($\log_{10}\eta_M \approx 19.0$ Pa · s and $\log_{10}\eta_K = 21.0$ $Pa \cdot s$). The locations of these specific points are shown as white dots in Figure 2. The inset is a schematic diagram of the model geometry and rheology.

changes) at large distances (>1–2 fault lengths) away from the fault for decades after a large earthquake [*To et al.*, 2004; *Pollitz et al.*, 2003].

Many classes of viscoelastic models have been used to successfully explain postseismic observations after large earthquakes (vertically layered viscoelastic models with Maxwell [*Hearn et al.*, 2002; *Ryder et al.*, 2007], standard linear solid [*Ryder et al.*, 2007], Burgers (transient) [*Ryder et al.*, 2011], and power law rheologies [*Freed and Bürgmann*, 2004] and models incorporating viscous shear zones [*Hearn et al.*, 2002, 2009], among others). To our knowledge, across all three-dimensional models, only those incorporating Burgers rheologies [*Hetland*, 2006; *Meade et al.*, 2013; P. R. DeVries et al., Viscoelastic block models of the North Anatolian Fault: A unified earthquake cycle representation of pre- and postseismic geodetic observations, submitted to *Bulletin of the Seismological Society of America*, 2016] and weak shear zones [*Yamasaki et al.*, 2014; *Hearn and Thatcher*, 2015] have so far been used to explain both preearthquake and postearthquake data. Here we focus on the former class of models (Figure 1, inset).

However, regardless of assumed viscosity structure, many existing models of viscoelastic ΔCFS (hereinafter referred to as $\Delta CFS_{classic}$; Figures 1 and 2 (row 1)) after large earthquakes cannot easily explain both the timing and locations of subsequent triggered earthquakes. These studies [e.g., *Pollitz and Sacks*, 2002; *Lorenzo-Martín et al.*, 2006] examine the predicted evolution of stress due to the effects of a single earthquake (Figure 2) or earthquake series. A simple extension of these models to multiple earthquake cycles is unphysical (Figure 1): repeated earthquakes on a given fault segment would incrementally increase the stress within the crust with each successive event, leading to runaway stresses over many earthquake cycles (Figure 1).

Here we present a kinematically consistent model of the viscoelastic perturbation to the stress in the crust over an arbitrary number of periodic earthquake cycles [*Pollitz and Schwartz*, 2008], based on a viscoelastic block model framework [e.g., *Sato and Matsu'ura*, 1988; *Hilley et al.*, 2009; *Chuang and Johnson*, 2011; *Hearn et al.*, 2013; *Tong et al.*, 2014; P. R. DeVries et al., submitted manuscript, 2016]. A kinematically consistent framework for viscoelastic earthquake cycle stress was previously applied to probabilistic seismic hazard estimation in the San Francisco Bay Area [*Pollitz and Schwartz*, 2008]. We determine the sensitivity of these models to changes in assumed viscosity structure and earthquake recurrence intervals. For simplicity, we limit our analysis and discussion to an idealized two-layer rheology structure (schizosphere and plastosphere) with a Burgers rheology in the lower layer (Figure 1, inset), but the kinematically consistent model framework is general and would apply to more complicated geometries and rheologies. We infer that earthquakes triggered by viscoelastic earthquake cycle effects may be most likely to occur during the first 50% of the earthquake cycle regardless of the assumed long-term and transient viscosities.

2. Kinematically Consistent Block Model Framework

In three-dimensional kinematically consistent viscoelastic block models [*Smith and Sandwell*, 2006; *Hilley et al.*, 2009; *Chuang and Johnson*, 2011; *Hearn et al.*, 2013; *Sato and Matsu'ura*, 1988; P. R. DeVries et al., submitted manuscript, 2016], interseismic velocities $\mathbf{v}_I$ are modeled as the sum of five components: $\mathbf{v}_B$, the

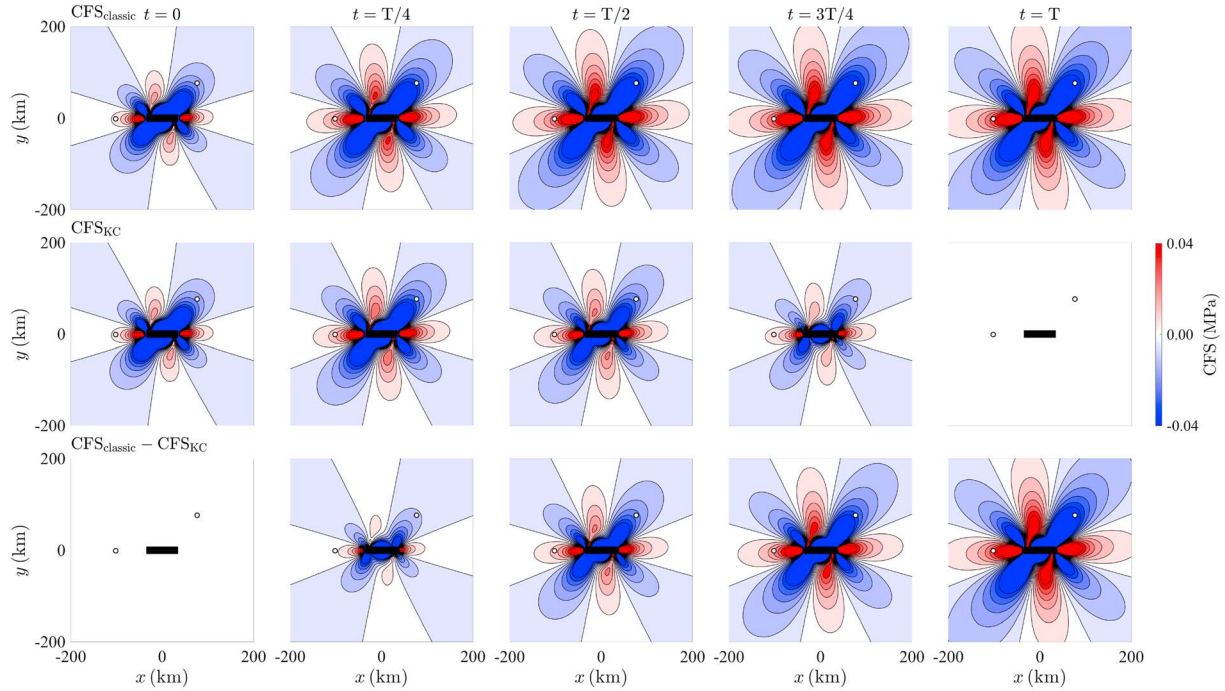

Figure 2. Comparison of (row 1) $\Delta CFS_{classic}$ and (row 2) ΔCFS_{KC} evaluated on faults parallel to the main rupture plane (in black) at equally spaced times through the earthquake cycle at 10 km depth for the same model as Figure 1. (row 3) To emphasize the phenomenological differences between the quantities, $\Delta CFS_{classic} - \Delta CFS_{KC}$ is shown.

velocities due to rigid block motion; $\mathbf{v}_{SD}$, the velocities due to the accumulated slip deficit; $\mathbf{v}_{\dot{\varepsilon}}$, the velocities due to internal strain of blocks; $\mathbf{v}_{VE}$, the viscoelastic effect of the most recent earthquake; and $\overline{\mathbf{v}}_{VE}$, the mean velocity throughout the earthquake cycle.

$$\mathbf{v}_I = \mathbf{v}_B - \mathbf{v}_{SD} + \mathbf{v}_{\dot{\varepsilon}} + \mathbf{v}_{VE}\left(\eta_M, \eta_K, t - t_{eq}\right) - \overline{\mathbf{v}}_{VE}(\eta_M, \eta_K, T) \tag{2}$$

The term $\mathbf{v}_{VE}(\eta_M, \eta_K, t - t_{eq})$ depends on the time since the most recent earthquake $t - t_{eq}$ and the Maxwell, η_M, and Kelvin, η_K, viscosities. We are here considering the interseismic motions during the earthquake cycle contributed by one fault with assumed recurrence interval T, but this framework can be easily generalized to multiple faults.

The viscoelastic block model framework in equation (2) ensures that over many earthquake cycles, the displacements everywhere are equal to the long-term block displacements. In classic block theory [*Matsu'ura et al.*, 1986; *McCaffrey*, 2002; *Meade and Hager*, 2005; *Meade and Loveless*, 2009], this is referred to as kinematic consistency.

3. Models of Kinematically Consistent Earthquake Cycle Stress

An analogous formulation of kinematically consistent stress [*Pollitz and Schwartz*, 2008] at a given location through the earthquake cycle may be derived from equation (2). (For simplicity we will assume that $t_{eq} = 0$, but solutions for $t_{eq} \neq 0$ may be easily found by substituting $t - t_{eq}$ for t in all subsequent equations.) Integrating equation (2) to find an expression for time-dependent interseismic displacement $\mathbf{D}_I(t)$,

$$\mathbf{D}_I(t) = \mathbf{v}_B t - \mathbf{v}_{SD} t + \mathbf{v}_{\dot{\varepsilon}} t + \mathbf{D}_{VE}(\eta_M, \eta_K, t) - \overline{\mathbf{v}}_{VE}(\eta_M, \eta_K)\, t \tag{3}$$

where $\mathbf{D}_{VE}(\eta_M, \eta_K, t)$ is the displacement due to the viscoelastic effects of the most recent earthquake at time t. We can now write an analogous expression for kinematically consistent time-dependent interseismic stress:

$$\boldsymbol{\sigma}_I(t) = \dot{\boldsymbol{\sigma}}_B t - \dot{\boldsymbol{\sigma}}_{SD} t + \dot{\boldsymbol{\sigma}}_{\dot{\varepsilon}} t + \boldsymbol{\sigma}_{VE}(\eta_M, \eta_K, t) - \dot{\overline{\boldsymbol{\sigma}}}_{VE}(\eta_M, \eta_K)\, t \tag{4}$$

Here $\boldsymbol{\sigma}_{VE}(\eta_M, \eta_K, t)$ is the stress due to the combined coseismic and viscoelastic effects of the most recent earthquake at time t. Because block motions are rigid rotations on the surface of the Earth in this block

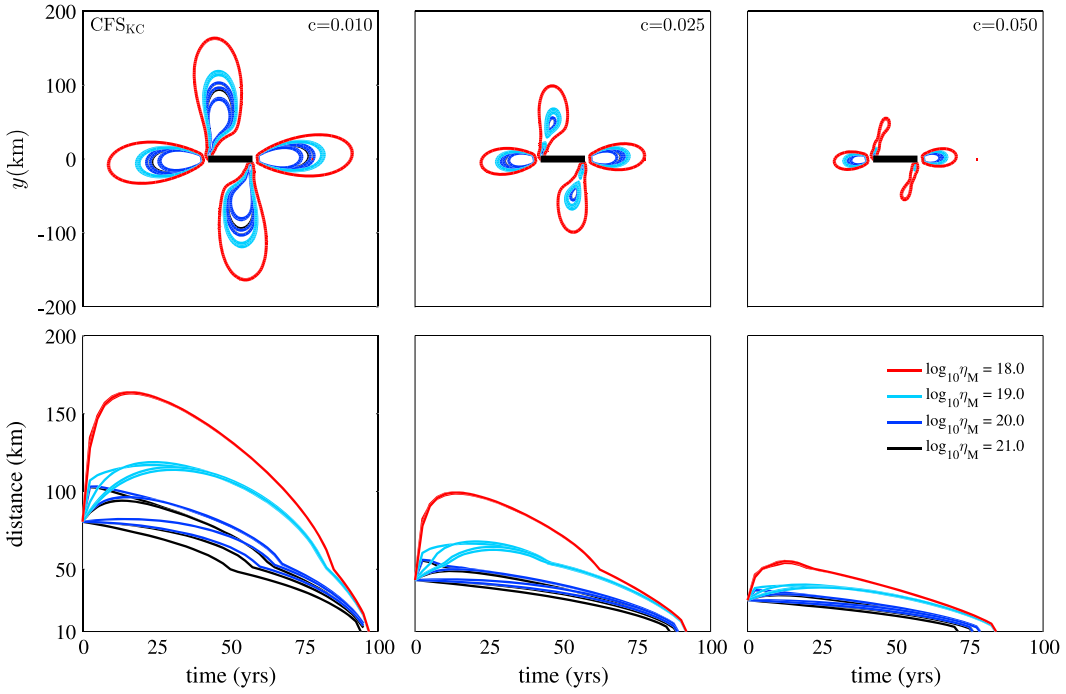

Figure 3. (row 1) The maximum size (measured by maximum distance from the fault) of lobes of stress (ΔCFS_{KC}) of different magnitudes ($c = 0.01$ MPa, $c = 0.025$ MPa, and $c = 0.05$ MPa) for all rheologies considered and $T = 100$ years. (row 2) The evolution of the maximum size (measured by maximum distance from the fault) of these lobes over time.

model framework, the associated stressing rate $\dot{\boldsymbol{\sigma}}_B = 0$. Here we will consider the simple case in which the internal strain rate $\dot{\boldsymbol{\sigma}}_{\dot{\varepsilon}}$ is zero everywhere, but this term may easily be incorporated in the following derivation. In addition, we can rewrite $\dot{\bar{\boldsymbol{\sigma}}}_{VE}(\eta_M, \eta_K)$ as $\frac{(\boldsymbol{\sigma}_{VE}(\eta_M,\eta_K,T)-\boldsymbol{\sigma}_{VE}(\eta_M,\eta_K,0))}{\bar{T}}$ because $\dot{\bar{\boldsymbol{\sigma}}}_{VE}$ depends only on η_M, η_K, and recurrence interval T,

$$\boldsymbol{\sigma}_I(t) = -\dot{\boldsymbol{\sigma}}_{SD}t + \boldsymbol{\sigma}_{VE}(\eta_M, \eta_K, t) - \frac{\boldsymbol{\sigma}_{VE}(\eta_M, \eta_K, T) - \boldsymbol{\sigma}_{VE}(\eta_M, \eta_K, 0)}{T}t \tag{5}$$

Because by definition $\dot{\boldsymbol{\sigma}}_{SD} = \frac{\boldsymbol{\sigma}_{VE}(\eta_M,\eta_K,0)}{T}$, we can obtain a concise expression for kinematically consistent interseismic stress evolution:

$$\boldsymbol{\sigma}_I(t) = \boldsymbol{\sigma}_{VE}(\eta_M, \eta_K, t) - \left[\frac{\boldsymbol{\sigma}_{VE}(\eta_M, \eta_K, T)}{T}\right]t \tag{6}$$

From equation (6), it is clear that at the end of the earthquake cycle $\boldsymbol{\sigma}_I(t = T) = 0$. As a result, kinematically consistent stress may reach a local maximum or minimum interseismically.

The terms in equations (6) can be calculated using a spectral propagator matrix method for calculating stresses, strains, and displacements due to point source dislocations in a vertically layered elastic medium [*Sato*, 1971; *Sato and Matsu'ura*, 1973, 1988; *Matsu'ura and Sato*, 1975, 1989; *Fukahata and Matsu'ura*, 2005, 2006; *Hashima et al.*, 2014]. The correspondence principle [e.g., *Nur and Mavko*, 1974; *Savage and Prescott*, 1978; *Hetland and Hager*, 2005; *de Hoog et al.*, 1982; *Hollenbeck*, 1998] is then used to calculate the time evolution of stresses due to viscoelastic effects. To approximate finite rupture sources accurately to within ~10 km of the fault surface, point sources are integrated according to a two-dimensional Legendre-Gaussian quadrature rule [e.g., *Hildebrand*, 1956].

We assume an idealized two-layer rheology structure, in which the upper elastic layer is 15 km thick and periodic earthquakes (with 1 m slip, length of fault $L = 60$ km, and therefore $M_w \approx 7.0$) rupture through this entire layer (Figure 1, inset). To isolate the effects of this fault segment, the rest of the fault is not locked

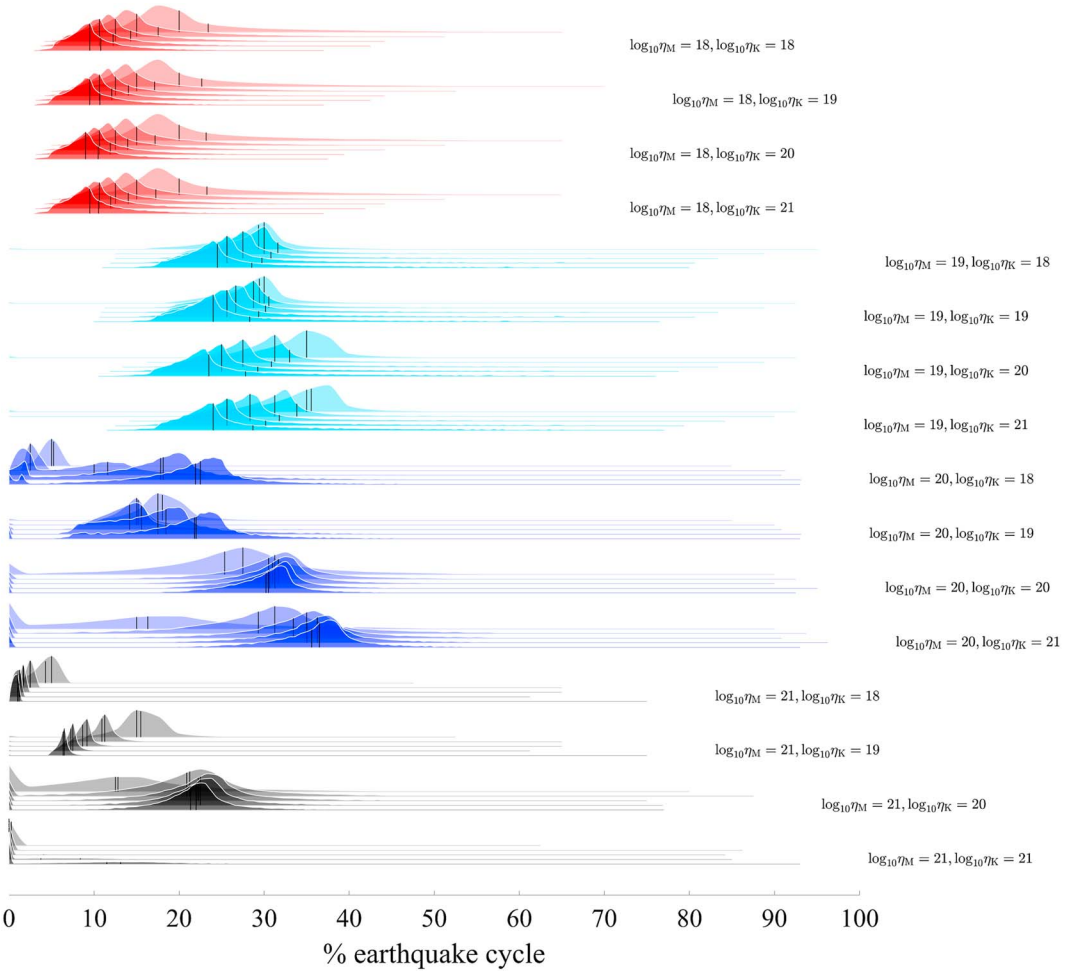

Figure 4. Histograms of the individual times t_p^{max} (in percent of earthquake cycle), at which points in an area 250 × 250 km around the fault at 10 km depth reach a maximum value of $\Delta CFS_{KC} > 0.0001$ MPa. The thin black vertical lines represent the mean time across all points for which t_p^{max} is defined ($\langle t_p^{max} \rangle$, see text) and the median time, med$\left(t_p^{max}\right)$. Opacity encodes recurrence intervals (T): the most transparent histograms (background) correspond to $T = 100$ years and the least transparent histograms correspond to $T = 500$ years.

interseismically in this model and therefore does not contribute to earthquake cycle stresses. Elastic moduli of $\lambda = \mu = 3 \times 10^{10}$ Pa are assumed in the elastic layer and in the Burgers viscoelastic layer. We examine the phenomenology of these models (Figures 1–4) for viscosities $\log_{10}\eta_M = 18.0 - 21.0$ Pa · s and $\log_{10}\eta_K = 18.0 - 21.0$ Pa · s in the lower layer and recurrence intervals T between 50 and 500 years.

4. Results

The differences between kinematically consistent models of earthquake cycle stress [*Pollitz and Schwartz*, 2008] and previous (or "classic") models of time-dependent stress after large earthquakes [e.g., *Freed and Lin*, 2001; *Zeng*, 2001; *Pollitz and Sacks*, 2002] are most easily understood by examining stress evolution at specific locations (Figure 1). Here ΔCFS will be evaluated on faults parallel to the main fault (Figure 2). After a single earthquake, at a given distance from the fault, values of $\Delta CFS_{classic}$ approach constant values (e.g., ~0.03 MPa at 70 km from the fault at 10 km depth for a two-layer Burgers model with $\log_{10}\eta_M = 19.0$ Pa · s and $\log_{10}\eta_K = 21.0$ Pa · s; Figure 1) long after the earthquake, as stresses slowly equilibrate through the crust. With each subsequent earthquake, the magnitudes of $\Delta CFS_{classic}$ increase incrementally and without bound (Figure 1). By contrast, in kinematically consistent models of Coulomb failure stress (ΔCFS_{KC}), the total stress

perturbation at the end of the earthquake cycle is zero, ensuring that earthquake-generated stresses in the crust do not increase indefinitely over many earthquake cycles (Figure 1) at any location. As a result, earthquake-generated stresses at locations near the fault may reach an absolute maximum (e.g., ~0.016 MPa at a point 70 km from the fault at 10 km depth for a two-layer Burgers model with $\log_{10}\eta_M = 19.0$ Pa · s, $\log_{10}\eta_K = 21.0$ Pa · s, and recurrence interval $T = 100$ years; Figure 1) during the interseismic period, before decaying to satisfy the kinematic consistency constraint. Below, we summarize a few more of the phenomenologically novel aspects of the model results (Figures 1–4) at a representative seismogenic depth of 10 km.

1. A geometric approach to understanding the phenomenology of these models is to examine the spatial extent of lobes of positive stress, defined as the areas with ΔCFS_{KC} greater than a certain threshold value (e.g., 0.01 MPa, 0.025 MPa, and 0.05 MPa; Figure 3). Although smaller stress changes (< 0.01 MPa) may be correlated with patterns of earthquakes in some cases [e.g., *Harris and Simpson*, 1996; *Deng and Sykes*, 1997a, 1997b; *Nalbant et al.*, 1998], these correlations may not be statistically significant [*Harris*, 1998]. Immediately after the earthquake, lobes of $\Delta CFS_{KC} > 0.01$ MPa extend up to 81 km at a depth of 10 km from the fault surface due to elastic stress changes alone; these lobes may gradually increase in size due to viscoelastic relaxation, before shrinking to maintain kinematic consistency (e.g., Figure 3). Here we measure lobe size by the farthest distance from the fault reached by the lobes, but a similar analysis using total area makes little difference to the results.

   At 10 km depth, the maximum extent of three lobes ($\Delta CFS_{KC} > 0.01$ MPa, $\Delta CFS_{KC} > 0.025$ MPa, and $\Delta CFS_{KC} > 0.05$ MPa) is largest (up to 164 km, 99 m, and 55 km from the fault and ~19,100 km^2, ~6860 km^2, and ~1960 km^2 in area, respectively, for $T = 100$ years; Figure 3) for low Maxwell ($\log_{10}\eta_M = 18.0$ Pa · s) viscosities. Variations in Kelvin viscosity have a negligible (<2 km) effect on the maximum extent of these lobes. For midrange Maxwell viscosities ($\log_{10}\eta_M = 19.0$ Pa · s) at $T = 100$ years, variations in Kelvin viscosity have a slightly larger effect (up to ~6 km) on maximum lobe sizes (Figure 3). Finally, at high Maxwell viscosities ($\log_{10}\eta_M = 20.0 - 21.0$ Pa · s) at $T = 100$ years, variations in Kelvin viscosity have a significant effect on maximum lobe size: lobes of $\Delta CFS_{KC} > 0.01$ MPa extend up to ~27% farther from the fault than an elastic model for low Kelvin viscosities ($\log_{10}\eta_K = 18.0 - 19.0$ Pa · s), but at high Kelvin viscosities ($\log_{10}\eta_K = 21.0$ Pa · s), the lobes never extend farther than an elastic model (Figure 3). These patterns hold true for higher stress thresholds (0.025 MPa and 0.05 MPa). Furthermore, quintupling the recurrence interval from $T = 100$ years to $T = 500$ years has a relatively modest effect on the results and trends discussed above: the maximum extents of lobes of $\Delta CFS_{KC} > 0.01$ MPa, 0.025 MPa, and 0.05 MPa increase by ~0–34% across all viscosities.
2. The evolution of these lobes of stress over time through the earthquake cycle—in particular the times at which lobes of stress reach their maximum extent—may be particularly relevant for the timing and spatial extent of viscoelastically triggered earthquakes. Across recurrence intervals from 50 to 500 years, lobes of $\Delta CFS_{KC} > 0.01$ MPa reach their maximum extent between 8% (at $T = 500$ years) and 20% (at $T = 50$) through the earthquake cycle for $\log_{10}\eta_M = 18.0$ Pa · s, regardless of Kelvin viscosity. For a slightly higher Maxwell viscosity ($\log_{10}\eta_M = 19.0$ Pa · s), lobes of $\Delta CFS_{KC} > 0.01$ MPa reach their maximum extent 15–30% through the earthquake (variations in assumed recurrence interval and Kelvin viscosity may affect this timing by up to 10% and 15%, respectively). For even higher viscosities, lobes of $\Delta CFS_{KC} > 0.01$ MPa reach their maximum extent ~0–31% through the earthquake cycle for $\log_{10}\eta_M = 20.0$ Pa · s and ~0–18% of the earthquake cycle for $\log_{10}\eta_M = 21.0$ Pa · s. These trends are similar for other lobe thresholds as well (e.g., 0.025 MPa and 0.05 MPa).
3. Finally, we can also look at the evolution of stress at individual locations around the fault over time for a more nuanced understanding of the model behavior (Figure 4). Here we will define the time t_p^{max} to be the time (in units of percent through the earthquake cycle) at which a point p near the fault experiences an absolute (positive) maximum $\Delta CFS_{KC} > 0.0001$ MPa. With this definition, it is clear that t_p^{max} may be 0 at many locations for high viscosities (Figure 3). For low Maxwell viscosities ($\log_{10}\eta_M = 18.0$ Pa · s) across recurrence intervals between 100 and 500 years, the mean time, at which points (in an area 250×250 around the 60 km long fault at 10 km depth at points spaced ~2.5 km apart) experience an absolute maximum $\Delta CFS_{KC} > 0.0001$ MPa, or $\left\langle t_p^{max} \right\rangle$, is ~11–25% through the earthquake cycle. For slightly higher Maxwell viscosities ($\log_{10}\eta_M = 19.0$ Pa · s), $\left\langle t_p^{max} \right\rangle = 30 - 35\%$, and at the highest Maxwell viscosities ($\log_{10}\eta_M = 20.0 - 21.0$ Pa · s), the effects of Kelvin viscosity and recurrence interval are more significant, leading to larger ranges (0–36%) in $\left\langle t_p^{max} \right\rangle$ (Figure 4).

5. Discussion

Kinematically consistent models of stress evolution [*Pollitz and Schwartz*, 2008] could have important implications for earthquake-triggering studies, because a viscoelastically triggered earthquake may be most likely to occur at a point p at time $t_p^{\max}$, when that point experiences the highest stress during the interseismic period. More generally, earthquakes triggered by viscoelastic earthquake cycle effects may be most numerous and geographically widespread during the periods of the earthquake cycle at which the extent of lobes of stress is largest. In kinematically consistent models, these stress maxima are easily identified in time and space.

From a practical standpoint, we may be most interested in a subset of the suite of models examined in this paper, because unified models of postseismic and interseismic data [e.g., *Hetland*, 2006; *Meade et al*., 2013; P. R. DeVries et al., submitted manuscript, 2016] require relatively low viscosities ($\sim 10^{18} - 10^{20}$ Pa · s) to explain all the available geodetic data. In two dimensions, the pre-earthquake and post-earthquake data from the 1999 $M_w = 7.4$ Izmit earthquake in Turkey may be explained by a two-layer Burgers model with a transient (Kelvin) relaxation time scale $\left(\tau_K = \frac{\eta_K}{\mu_K}\right)$ of 2–5 years and a long-term (Maxwell) time scale $\left(\tau_M = \frac{\eta_M}{\mu_M}\right)$ of over 400 years [*Hetland*, 2006]. The postseismic GPS velocity field from the Izmit earthquake has also been modeled with a combination of stable frictional afterslip and viscoelastic deformation with a Maxwell rheology with a viscosity of $2 - 5 \times 10^{19}$ Pa · s [*Hearn et al*., 2009]. These authors discuss how a Burgers model with two viscosities ($2 - 5 \times 10^{19}$Pa · s and 2×10^{20} Pa · s) might be required [*Hearn et al*., 2009] to explain geodetic observations from both before and after the earthquake. More recently, with a two-layer structure and a Burgers rheology (with Maxwell viscosity $\log_{10}\eta_M \approx 18.6 - 19.0$ Pa · s and Kelvin viscosity $\log_{10}\eta_K \approx 18.0 - 19.0$ Pa · s), a block model that incorporates tectonic plate motions, interseismic elastic strain accumulation, transient viscoelastic perturbations, and internal strain was found to explain both the pre-Izmit and post-Izmit earthquake observations with a single unified model (P. R. DeVries et al., submitted manuscript, 2016).

Together, these studies suggest that models with $\log_{10}\eta_K \leq 19.0$ Pa · s and $\log_{10}\eta_M \leq 20.0$ Pa · s may be able to explain all the available geodetic data from the earthquake cycle. Based on the evolution of kinematically consistent stress for these viscosity structures (Figures 3 and 4), we can make some broad observations about the potential likelihood of viscoelastically triggered earthquakes:

1. The spatial extent of earthquakes triggered by viscoelastic earthquake cycle effects may change over time, reaching a maximum between ~0 and 31% through the earthquake cycle (Figure 3).
2. Despite complex behavior at certain viscosities, the mean times at which points reach an absolute (positive) maximum $\Delta CFS_{KC} > 0.0001$ MPa is less than 40% through the earthquake cycle across all viscosities and recurrence intervals. Thus, based on these models, although individual points do reach an absolute maximum values of ΔCFS_{KC} as late as 95% through the earthquake cycle (Figure 4), we might—albeit simplistically—expect most earthquakes triggered by viscoelastic earthquake cycle effects to occur in the first half of the earthquake cycle.

Of course, these observations are based on many simplifying assumptions: a periodic earthquake cycle on a single fault segment and no secondary triggering effects [e.g., *Meier et al*., 2014; *Michael and Jones*, 1998; *Felzer et al*., 2002, 2003; *Helmstetter*, 2003; *Helmstetter et al*., 2005; *Marsan*, 2003]. Additional earthquake cycle effects from adjacent fault segments could dramatically affect patterns of stress evolution. Perhaps most fundamentally, we are also assuming that the magnitude of stress at a given time is the only factor that influences the likelihood of a triggered earthquake (in other words, we ignore potential secondary processes like rate and state friction [e.g., *Dieterich*, 1979], subcritical crack growth [*Atkinson*, 1984], or transient increases in pore pressure [e.g., *Hill et al*., 1993; *Brodsky et al*., 2003; *Brodsky and Prejean*, 2005]). Despite these significant assumptions, the observations listed above effectively summarize both the behavior and the potential implications of these kinematically consistent models.

A central result of this paper is that kinematically consistent viscoelastic earthquake cycle models make distinctly different predictions from classic conceptions of time-dependent viscoelastic stress evolution. Without a known absolute failure threshold (and a dependable measure of the full state of stress in the crust), it is difficult to identify a time at which earthquakes triggered by viscoelastic earthquake cycle effects would

be most likely based on classic models (Figure 1). This challenge does not exist for kinematically consistent models presented here (equations (6) and Figures 1–4), in which the spatial extent of lobes of stress in these models—and the magnitudes of stress in the volume surrounding the fault—must reach a maximum either immediately after or at sometime during the earthquake cycle (Figure 4). For these kinematically consistent models, we may simply base inferences about the timing of viscoelastically triggered earthquakes on the timing of stress maxima (Figures 3 and 4), rather than on any arbitrary or empirically constrained stress thresholds.

6. Conclusion

In a kinematically consistent block model framework, over many earthquake cycles, the displacements everywhere are equal to the long-term block displacements. Here we present an analogous framework for viscoelastic stress through the earthquake cycle. These models can be distinguished phenomenologically from previously existing models of stress after large earthquakes in two significant ways: the total stress perturbation at the end of the earthquake cycle is zero, and as a result, earthquake-generated stresses in these models may reach an absolute maximum during the interseismic period. Based on these models of kinematically consistent stress, we might expect that (1) the spatial extent of earthquakes triggered by viscoelastic earthquake cycle effects may change over time, reaching a maximum between ~0 and 31% through the earthquake cycle, and (2) the vast majority of viscoelastically triggered earthquakes may occur during the first half of the interseismic period.

Acknowledgments
We thank Roland Bürgmann, Fred Pollitz, and Editor Andrew Newman for their thoughtful reviews that led to substantial improvements. No data were used in producing the results in this manuscript. All data referred to in the discussion are properly cited and referred to in the reference list. This work was supported by Harvard University, the Southern California Earthquake Center (contribution 6239) funded by NSF Cooperative Agreement EAR-1033462 and USGS Cooperative Agreement G12AC20038, and the Department of Energy Computational Science Graduate Fellowship Program of the Office of Science and National Nuclear Security Administration in the Department of Energy under contract DE-FG02-97ER25308.

References

Atkinson, B. K. (1984), Subcritical crack growth in geological materials, *J. Geophys. Res.*, *89*, 4077–4114, doi:10.1029/JB089iB06p04077.
Brodsky, E. E., and S. G. Prejean (2005), New constraints on mechanisms of remotely triggered seismicity at Long Valley Caldera, *J. Geophys. Res.*, *110*, B04302, doi:10.1029/2004JB003211.
Brodsky, E. E., E. Roeloffs, D. Woodcock, I. Gall, and M. Manga (2003), A mechanism for sustained groundwater pressure changes induced by distant earthquakes, *J. Geophys. Res.*, *108*(B8), 2390, doi:10.1029/2002JB002321.
Chuang, R. Y., and K. M. Johnson (2011), Reconciling geologic and geodetic model fault slip-rate discrepancies in Southern California: Consideration of nonsteady mantle flow and lower crustal fault creep, *Geology*, *39*(7), 627–630.
de Hoog, F. R., J. H. Knight, and A. N. Stokes (1982), An improved method for numerical inversion of Laplace transforms, *SIAM J. Sci. Stat. Comput.*, *3*(3), 357–366.
Deng, J., and L. R. Sykes (1997a), Evolution of the stress field in Southern California and triggering of moderate-size earthquakes: A 200-year perspective, *J. Geophys. Res.*, *102*, 9859–9886, doi:10.1029/96JB03897.
Deng, J., and L. R. Sykes (1997b), Stress evolution in Southern California and triggering of moderate-, small-, and micro-size earthquake, *J. Geophys. Res.*, *102*, 24,411–24,435, doi:10.1029/97JB02127.
Dieterich, J. H. (1979), Modeling of rock friction: 1. Experimental results and constitutive equations, *J. Geophys. Res.*, *84*, 2161–2168, doi:10.1029/JB084iB05p02161.
Dieterich, J. H. (1992), Earthquake nucleation on faults with rate-and state-dependent strength, *Tectonophysics*, *211*(1), 115–134.
Dieterich, J. H. (1994), A constitutive law for rate of earthquake production and its application to earthquake clustering, *J. Geophys. Res.*, *99*, 2601–2618, doi:10.1029/93JB02581.
Doser, D. I., and R. Robinson (2002), Modeling stress changes induced by earthquakes in the southern Marlborough region, South Island, New Zealand, *Bull. Seismol. Soc. Am.*, *92*(8), 3229–3238.
Felzer, K. R., T. W. Becker, R. E. Abercrombie, G. Ekstrom, and J. R. Rice (2002), Triggering of the 1999 M_w 7.1 Hector Mine earthquake by aftershocks of the 1992 M_w 7.3 Landers earthquake, *J. Geophys. Res.*, *107*(B9), 2190, doi:10.1029/2001JB000911.
Felzer, K. R., R. E. Abercrombie, and G. Ekström (2003), Secondary aftershocks and their importance for aftershock prediction, *Bull. Seismol. Soc. Am.*, *93*(4), 1433–1448.
Freed, A. M., and R. Bürgmann (2004), Evidence of power law flow in the Mojave desert mantle, *Nature*, *430*, 548–551.
Freed, A. M., and J. Lin (2001), Delayed triggering of the 1999 Hector Mine earthquake by viscoelastic stress transfer, *Nature*, *411*(6834), 180–183.
Fukahata, Y., and M. Matsu'ura (2005), General expressions for internal deformation fields due to a dislocation source in a multilayered elastic half-space, *Geophys. J. Int.*, *161*(2), 507–521.
Fukahata, Y., and M. Matsu'ura (2006), Quasi-static internal deformation due to a dislocation source in a multilayered elastic/viscoelastic half-space and an equivalent theorem, *Geophys. J. Int.*, *166*(1), 418–432.
Hardebeck, J. L., J. J. Nazareth, and E. Hauksson (1998), The static stress change triggering model: Constraints from two Southern California aftershock sequences, *J. Geophys. Res.*, *103*, 24,427–24,437, doi:10.1029/98JB00573.
Harris, R. A. (1998), Introduction to special section: Stress triggers, stress shadows, and implications, *J. Geophys. Res.*, *103*, 24,347–24,358, doi:10.1029/98JB01576.
Harris, R. A., and R. W. Simpson (1996), In the shadow of 1856: The effect of the Great Ft. Tejon earthquake on subsequent earthquakes in Southern California, *Geophys. Res. Lett.*, *23*, 229–232, doi:10.1029/96GL00015.
Hashima, A., M. Fukahata, C. Hashimoto, and M. Matsu'ura (2014), Quasi-static strain and stress fields due to a moment tensor in elastic–viscoelastic layered half-space, *Pure Appl. Geophys.*, *171*(8), 1669–1693.
Hearn, E. H., and W. R. Thatcher (2015), Reconciling viscoelastic models of postseismic and interseismic deformation: Effects of viscous shear zones and finite-length ruptures, *J. Geophys. Res. Solid Earth*, *120*, 2794–2819, doi:10.1002/2014JB011361.

Hearn, E. H., R. Bürgmann, and R. E. Reilinger (2002), Dynamics of Izmit earthquake postseismic deformation and loading of the Düzce earthquake hypocenter, *Bull. Seismol. Soc. Am.*, *92*(1), 172–193.
Hearn, E. H., S. McClusky, S. Ergintav, and R. E. Reilinger (2009), Izmit earthquake postseismic deformation and dynamics of the North Anatolian Fault Zone, *J. Geophys. Res.*, *114*, B08405, doi:10.1029/2008JB006026.
Hearn, E. H., C. T. Onishi, F. F. Pollitz, and W. R. Thatcher (2013), How do "ghost transients" from past earthquakes affect GPS slip rate estimates on Southern California faults?, *Geochem. Geophys. Geosyst.*, *14*, 828–838, doi:10.1002/ggge.20080.
Helmstetter, A. (2003), Is earthquake triggering driven by small earthquakes?, *Phys. Rev. Lett.*, *91*(5), 058501.
Helmstetter, A., Y. Y. Kagan, and D. D. Jackson (2005), Importance of small earthquakes for stress transfer and earthquake triggering, *J. Geophys. Res.*, *110*, B05S08, doi:10.1029/2004JB003286.
Hetland, E. (2006), Models of interseismic deformation with an analytic framework for the inclusion of general linear viscoelastic rheologies, PhD thesis, 255 pp., Mass. Inst. of Technol.
Hetland, E., and B. H. Hager (2005), Postseismic and interseismic displacements near a strike-slip fault: A two-dimensional theory for general linear viscoelastic rheologies, *J. Geophys. Res.*, *110*, B10401, doi:10.1029/2005JB003689.
Hildebrand, F. B. (1956), *Introduction to Numerical Analysis*, 2nd, 704 pp. ed., Dover, Mineola, N. Y. [Reprinted 1987].
Hill, D. P., et al. (1993), Seismicity remotely triggered by the magnitude 7.3 Landers, California, earthquake, *Science*, *260*(5114), 1617–1623.
Hilley, G. E., K. M. Johnson, M. Wang, Z.-K. Shen, and R. Bürgmann (2009), Earthquake-cycle deformation and fault slip rates in northern Tibet, *Geology*, *37*(1), 31–34.
Hollenbeck, K. J. (1998), INVLAP.M: A MATLAB function for numerical inversion of Laplace transforms by the de Hoog algorithm. [Available at http://www.isva.dtu.dk/staff/karl/invlap.htm.]
King, G. C. P., and M. Cocco (2001), Fault interaction by elastic stress changes: New clues from earthquake sequences, *Adv. Geophys.*, *44*, 1–38.
King, G. C. P., R. S. Stein, and J. Lin (1994), Static stress changes and the triggering of earthquakes, *Bull. Seismol. Soc. Am.*, *84*(3), 935–953.
Lorenzo-Martín, F., F. Roth, and R. Wang (2006), Elastic and inelastic triggering of earthquakes in the North Anatolian Fault Zone, *Tectonophysics*, *424*(3), 271–289.
Marsan, D. (2003), Triggering of seismicity at short timescales following Californian earthquakes, *J. Geophys. Res.*, *108*(B5), 2266, doi:10.1029/2002JB001946.
Matsu'ura, M., and R. Sato (1975), Static deformation due to the fault spreading over several layers in a multi-layered medium. Part II: Strain and tilt, *J. Phys. Earth*, *23*(1), 1–29.
Matsu'ura, M., and T. Sato (1989), A dislocation model for the earthquake cycle at convergent plate boundaries, *Geophys. J. Int.*, *96*(1), 23–32.
Matsu'ura, M., D. D. Jackson, and A. Cheng (1986), Dislocation model for aseismic crustal deformation at Hollister, California, *J. Geophys. Res.*, *91*, 12,661–12,674, doi:10.1029/JB091iB12p12661.
McCaffrey, R. (2002), Crustal block rotations and plate coupling, in *Plate Boundary Zones*, *Geodyn. Ser.*, vol. 30, edited by S. Stein and J. Freymueller, pp. 101–122, AGU, Washington, D. C.
Meade, B. J., and B. H. Hager (2005), Block models of crustal motion in Southern California constrained by GPS measurements, *J. Geophys. Res.*, *110*, B03403, doi:10.1029/2004JB003209.
Meade, B. J., and J. P. Loveless (2009), Block modeling with connected fault-network geometries and a linear elastic coupling estimator in spherical coordinates, *Bull. Seismol. Soc. Am.*, *99*(6), 3124–3139.
Meade, B. J., Y. Klinger, and E. A. Hetland (2013), Inference of multiple earthquake cycle relaxation timescales from irregular geodetic sampling of interseismic deformation, *Bull. Seismol. Soc. Am.*, *103*(5), 2824–2835.
Meier, M.-A., M. J. Werner, J. Woessner, and S. Wiemer (2014), A search for evidence of secondary static stress triggering during the 1992 M_w 7.3 Landers, California, earthquake sequence, *J. Geophys. Res. Solid Earth*, *119*, 3354–3370, doi:10.1002/2013JB010385.
Michael, A. J., and L. M. Jones (1998), Seismicity alert probabilities at Parkfield, California, revisited, *Bull. Seismol. Soc. Am.*, *88*(1), 117–130.
Nalbant, S. S., A. Hubert, and G. C. King (1998), Stress coupling between earthquakes in northwest Turkey and the north Aegean Sea, *J. Geophys. Res.*, *103*, 24,469–24,486, doi:10.1029/98JB01491.
Nur, A., and G. Mavko (1974), Postseismic viscoelastic rebound, *Science*, *183*(4121), 204–206.
Parsons, T., and D. S. Dreger (2000), Static stress impact of the 1992 Landers earthquake sequence on nucleation and slip at the site of the 1999 $M = 7.1$ Hector Mine earthquake, Southern California, *Geophys. Res. Lett.*, *27*, 1949–1952, doi:10.1029/1999GL011272.
Pollitz, F., M. Vergnolle, and E. Calais (2003), Fault interaction and stress triggering of twentieth century earthquakes in Mongolia, *J. Geophys. Res.*, *108*(B10), 2503, doi:10.1029/2002JB002375.
Pollitz, F. F., and I. S. Sacks (2002), Stress triggering of the 1999 Hector Mine earthquake by transient deformation following the 1992 Landers earthquake, *Bull. Seismol. Soc. Am.*, *92*(4), 1487–1496.
Pollitz, F. F., and D. Schwartz (2008), Probabilistic seismic hazard in the San Francisco Bay Area based on a simplified viscoelastic-cycle model of fault interactions, *J. Geophys. Res.*, *113*, B05409, doi:10.1029/2007JB005227.
Ryder, I., B. Parsons, T. J. Wright, and G. J. Funning (2007), Post-seismic motion following the 1997 Manyi (Tibet) earthquake: InSAR observations and modeling, *Geophys. J. Int.*, *169*(3), 1009–1027.
Ryder, I., R. Bürgmann, and F. Pollitz (2011), Lower crustal relaxation beneath the Tibetan Plateau and Qaidam Basin following the 2001 Kokoxili earthquake, *Geophys. J. Int.*, *187*(2), 613–630.
Sato, R. (1971), Crustal deformation due to dislocation in a multi-layered medium, *J. Phys. Earth*, *19*(1), 31–46.
Sato, R., and M. Matsu'ura (1973), Static deformation due to the fault spreading over several layers in a multi-layered medium. Part I: Displacement, *J. Phys. Earth*, *21*(3), 227–249.
Sato, T., and M. Matsu'ura (1988), A kinematic model for deformation of the lithosphere at subduction zones, *J. Geophys. Res.*, *93*, 6410–6418, doi:10.1029/JB093iB06p06410.
Savage, J. C., and W. H. Prescott (1978), Asthenosphere readjustment and the earthquake cycle, *J. Geophys. Res.*, *83*, 3369–3376, doi:10.1029/JB083iB07p03369.
Simpson, R. W., and P. A. Reasenberg (1994), Earthquake-induced static stress changes on central California faults, in *The Loma Preita, California Earthquake of October 17, 1989—Tectonic Processes and Models*, *U.S. Geol. Surv. Prof. Pap. 1550-F*, edited by R. W. Simpson, pp. F55–F89.
Smith, B. R., and D. T. Sandwell (2006), A model of the earthquake cycle along the San Andreas fault system for the past 1000 years, *J. Geophys. Res.*, *111*, B01405, doi:10.1029/2005JB003703.
Steacy, S., J. Gomberg, and M. Cocco (2005), Introduction to special section: Stress transfer, earthquake triggering, and time-dependent seismic hazard, *J. Geophys. Res.*, *110*, B05S01, doi:10.1029/2005JB003692.
Stein, R. S., A. A. Barka, and J. H. Dieterich (1997), Progressive failure on the North Anatolian Fault since 1939 by earthquake stress triggering, *Geophys. J. Int.*, *128*(3), 594–604.

To, A., R. Bürgmann, and F. Pollitz (2004), Postseismic deformation and stress changes following the 1819 Rann of Kachchh, India earthquake: Was the 2001 Bhuj earthquake a triggered event?, *Geophys. Res. Lett.*, *31*, L13609, doi:10.1029/2004GL020220.

Tong, X., B. R. Smith-Konter, and D. T. Sandwell (2014), Is there are discrepancy between geological and geodetic slip rates along the San Andreas fault system?, *J. Geophys. Res. Solid Earth*, *119*, 2518–2538, doi:10.1002/2013JB010765.

Yamasaki, T., T. J. Wright, and G. A. Houseman (2014), Weak ductile shear zone beneath a major strike-slip fault: Inferences from earthquake cycle model constrained by geodetic observations of the western North Anatolian Fault Zone, *J. Geophys. Res. Solid Earth*, *119*, 3678–3699, doi:10.1002/2013JB010347.

Zeng, Y. (2001), Viscoelastic stress triggering of the 1999 Hector Mine earthquake by the 1992 Landers earthquake, *Geophys. Res. Lett.*, *28*, 3007–3010, doi:10.1029/2000GL012806.